PUBLISHED BY IOP PUBLISHING FOR SISSA

RECEIVED: *December 15, 2008*
ACCEPTED: *January 28, 2009*
PUBLISHED: *March 17, 2009*

PIXEL 2008 INTERNATIONAL WORKSHOP
FERMILAB, BATAVIA, IL, U.S.A.
23–26 SEPTEMBER 2008

Pixel detectors for x-ray imaging spectroscopy in space

J. Treis,[a,b,1] **R. Andritschke,**[a,c] **R. Hartmann,**[a,e] **S. Herrmann,**[a,c] **P. Holl,**[a,e] **T. Lauf,**[a,c] **P. Lechner,**[a,e] **G. Lutz,**[a,e] **N. Meidinger,**[a,c] **M. Porro,**[a,c] **R.H. Richter,**[a,d] **F. Schopper,**[a,c] **H. Soltau**[a,e] **and L. Strüder**[a,c]

[a] *MPI Semiconductor Laboratory, Otto-Hahn-Ring 6, D-81739 Munich, Germany*
[b] *Max-Planck-Institute for Solar Systems Research, Max-Planck-Straße 2, D-37191 Katlenburg-Lindau, Germany*
[c] *Max-Planck-Institute for Extraterrestrial Physics, Giessenbachstraße, D-85748 Garching, Germany*
[d] *Max-Planck-Institute for Physics, Föhringer Ring 6, D-80805 Munich, Germany*
[e] *PNSensor GmbH, Römerstraße 28, D-80803 Munich, Germany*

E-mail: jft@hll.mpg.de

ABSTRACT: Pixelated semiconductor detectors for X-ray imaging spectroscopy are foreseen as key components of the payload of various future space missions exploring the x-ray sky. Located on the platform of the new Spectrum-Roentgen-Gamma satellite, the eROSITA (extended Roentgen Survey with an Imaging Telescope Array) instrument will perform an imaging all-sky survey up to an X-ray energy of 10 keV with unprecedented spectral and angular resolution. The instrument will consist of seven parallel oriented mirror modules each having its own pnCCD camera in the focus. The satellite born X-ray observatory SIMBOL-X will be the first mission to use formation-flying techniques to implement an X-ray telescope with an unprecedented focal length of around 20 m. The detector instrumentation consists of separate high- and low energy detectors, a monolithic 128 $\times$ 128 DEPFET macropixel array and a pixellated CdZTe detector respectively, making energy

[1] Corresponding author.

doi:10.1088/1748-0221/4/03/P03012

band between 0.5 to 80 keV accessible. A similar concept is proposed for the next generation X-ray observatory IXO. Finally, the MIXS (Mercury Imaging X-ray Spectrometer) instrument on the European Mercury exploration mission BepiColombo will use DEPFET macropixel arrays together with a small X-ray telescope to perform a spatially resolved planetary XRF analysis of Mercury's crust. Here, the mission concepts and their scientific targets are briefly discussed, and the resulting requirements on the detector devices together with the implementation strategies are shown.

KEYWORDS: X-ray detectors and telescopes; Spectrometers; X-ray fluorescence (XRF) systems

2009 JINST 4 P03012

Contents

2009 JINST 4 P03012

1 Introduction

Imaging spectroscopy of ionizing radiation in the X-ray range targets the simultaneous detection of energy and interaction point of an X-ray photon with the detector material. Typical application is the field of X-ray astronomy, where space-born observatories carrying an X-ray optical system, e.g. Wolter Type X-ray telescopes, are combined with a dedicated focal plane instrumentation featuring varying kinds of X-ray detectors.

Especially in the energy range between ~ 100 eV and ~ 20 keV X-ray semiconductor detectors based on silicon planar technology increasingly find application as focal plane instrumentation for X-ray astronomy. Silicon shows an efficient absorbtion in the low energy X-ray band, and near Fano-limited X-ray spectroscopy is possible with silicon based devices at relatively moderate operating conditions. This can be achieved by integrating part of the readout electronics within the detector device, reducing the readout capacitance to the minimum extend possible, in combination with high performance, low noise readout systems. In addition, a variety of innovative device concepts can be used to conveniently optimize the detector design with respect to the requirements of the instrument, e.g. by tailoring the pixel size.

Common X-ray optical systems provide PSF sizes in in the range < 1 mm, so adapting the pixel size to the optics PSF is required to avoid charge splitting between pixels, which reduces the overall spectral resolution due to recombination noise, as well as unnecessary, power-costly oversampling of the PSF. Thus, optimized pixel sizes at the order of several hundreds of microns are desirable. This is difficult to combine with the demand of as good an energy resolution as possible, as for common pad detectors, for instance, the equivalent capacitance is coupled to the pixel area.

When using silicon as a detector device, the principle of sidewards depletion [1] offers a convenient and effective way to simultaneously adapt the pixel size of a focal plane array to the requirements of the imaging system and avoid deterioration of the sensor performance by decoupling

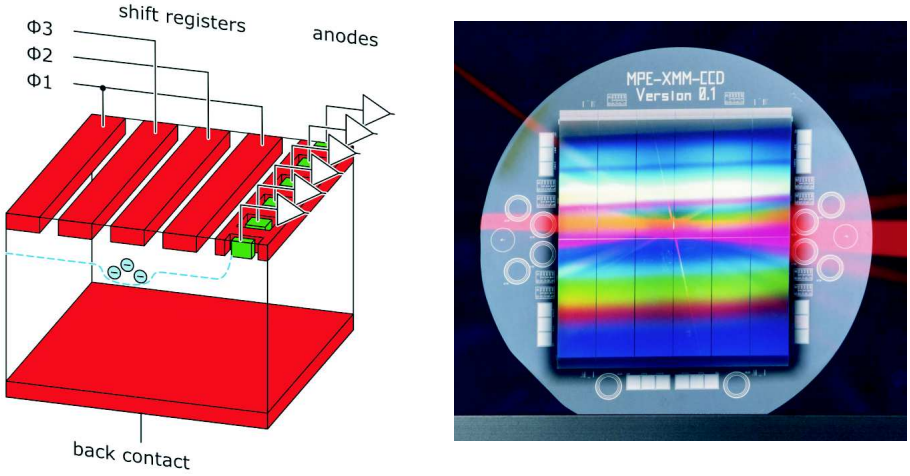

Figure 1. Cutaway of a pnCCD device (left). The charge is transferred through the transfer channel, which falls together with the potential minimum generated by sidewards depletion, located deep underneath the surface of the detector device. The potentials of the ϕ-pulses for the transfer of the charge are applied using the same p^+ implantations required for sidewards depletion. Column-parallel readout using an column-individual integrated JFET provides for fast processing of the data. In this way, wafer scale devices like the EPIC pnCCD on XMM Newton (right) have been built.

the sensitive area of the pixel from the capacitance of the readout node, which can be minimized by design. This yields extremely good readout noise performance. For X-ray detectors, noise performance is usually quantified in terms of electrons rms equivalent noise charge (ENC), rather than by a fixed signal to noise ratio, as the X-ray energy is variable. With sidewards depleted devices, noise figures of of 2-4 electrons ENC are regularly achieved. In addition, sidewards depleted devices are fully depleted, i.e. sensitive over the entire bulk thickness, and, if illuminated from the backside, can be provided with an extremely thin, homogeneous entrance window with a fill factor of 100% to meet the requirement of good quantum efficiency in both high and low energy range.

Pixelated, silicon based X-ray detectors based on the principle of sidewards depletion are currently being developed for a variety of space missions at the MPI semiconductor laboratory in Munich. The selected device concept strongly depends on the performance of the respective X-ray optics. While pnCCD detectors are suitable for detectors with pixel sizes smaller than $\sim 200\ \mu$m, larger requested pixel sizes require the use of new detector concepts, e.g. DEPFET based MPDs. Although these devices strongly differ in concept and properties, e.g. extend and internal mechanism of charge sharing between pixels [2, 3], they are equally suitable in terms of performance for the task of X-ray imaging spectroscopy. All devices require highly optimized low noise integrated readout electronics which allows high speed readout to avoid photon pileup. In the following, the device concepts are briefly introduced, and an outline of the respective missions together with the design drivers for the selection of the respective X-ray detector will be given.

1.1 X-ray pnCCDs

The X-ray pnCCD was the first integrating large area X-ray detector built using the principle of sidewards depletion [1]. By asymmetric biasing of the surfaces of a sidewards depleted bulk,

2009 JINST 4 P03012

the potential minimum is shifted under the top surface of the silicon bulk. The p^+-implantations located here are segmented and connected in a way that by clocking the voltages in the correct sequence a three phase transfer of the charge towards a column-individual readout anode is possible (see figure 1). This 'buried' transfer channel greatly increases the radiation tolerance of the device. As the backside is completely unstructured, it can be used as radiation entrance window, and with a thin backside implantation, extremely good QE values even in the low energy range can be achieved. Together with the tailored column-parallel readout electronics of the CAMEX type, readout noise figures of ~ 2 electrons ENC can be achieved. The pnCCD concept is a proven device technology for space applications. The largest sensor of this kind so far is the EPIC pnCCD device on ESA's XMM Newton X-ray observatory [4]. It is operating continuously since 1999 without any problem. The device has an overall area of 6×6 cm^2 with a pixel size of 150×150 μm^2, occupying nearly the entire usable area of an 4" silicon wafer. The device still delivers an effective readout noise of 6 electrons ENC and an energy resolution of 140 eV FWHM @ 5.9 keV. In the last years, the pnCCD technology has been continuously improved [5]; features like double sided, column parallel readout or frame store architecture have been developed for the next generation of pnCCD devices.

1.2 DEPMOSFET devices

A DEPMOSFET (DEpleted P-channel MOSFET) combined detector-amplifier structure consists of a p-channel MOSFET integrated on the surface of an n-type silicon bulk [6, 7]. Using the principle of sideways depletion, the bulk can be fully depleted. By applying appropriate bias potentials, a potential minimum for electrons can be generated below the transistor channel, and all bulk-generated electrons are collected there. Their presence modulates the charge carrier density in the channel in the same way as charge on the external gate, making the channel conductivity a function of the charge in the potential minimum, which is therefore also referred to as *internal gate*. The internal gate persists and keeps integrating charges regardless from the presence of a transistor current, so the transistor can be turned off during signal integration to reduce power consumption. The charge can be removed regularly by applying a positive voltage pulse to an n^+-doped region close to the internal gate, the *clear*-contact. The charge handling capacity of conventional DEPFETs is in the range of 10^5 e^-. The type of DEPMOSFET structures used for X-ray spectroscopy have circular transistor geometry. The *clear region* here consists of an additional N-MOSFET composed of the clear contact and a surrounding MOS structure, the *cleargate*. Figure 2 shows a cutaway of a circular DEPMOSFET structure.

Currently, DEPFET readout is mostly done using a source follower circuit, where the change in channel conductivity is converted into a voltage step at the DEPFET source. The signal is evaluated by correlated double sampling (CDS), i.e. sampling the source voltage levels before and after the clear and calculating the difference. In large FPA matrix devices, a pixel array is placed on a common bulk and back contact. As shown in figure 3, the pixels are interconnected for row-wise, column-parallel readout, i.e. the signal information of all pixel in a row is processed in parallel, and the whole matrix is read out in a rolling shutter mode [8]. In addition to its use as X-ray detector, the DEPFET concept is the basic working principle for a large variety of versatile innovative detector concepts [9].

2009 JINST 4 P03012

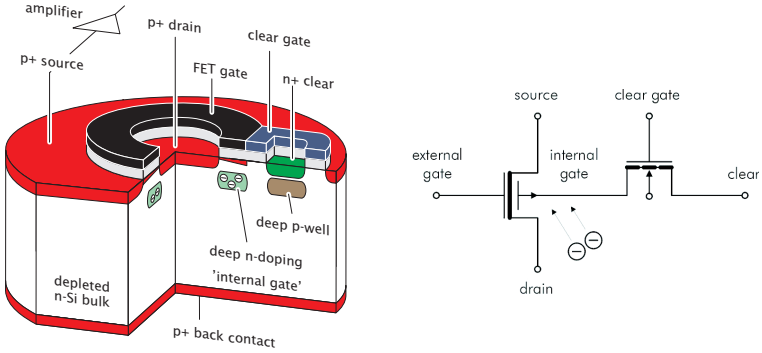

Figure 2. Cutaway of a circular DEPMOSFET pixel device and the equivalent circuit schematics: A MOSFET with two gates: External and Internal Gate, while the latter can be contacted via the n-type Clear-FET.

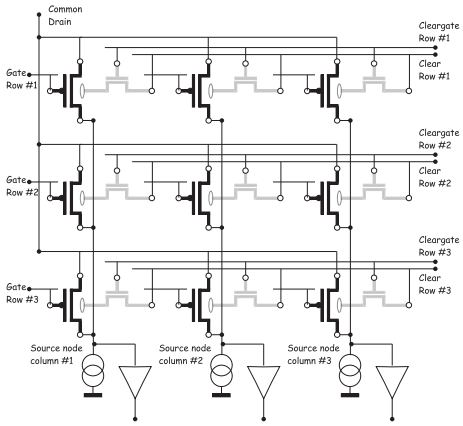

Figure 3. Schematic interconnection of DEPMOSFET matrix pixels for row-wise readout. Row-wise connection of Gate, Clear and Cleargate voltages provides for row addressing, and column-wise connection of the readout nodes provides for column-parallel readout.

For operating a matrix, a set of VLSI integrated control- and readout electronics is used. The control-ICs used are multichannel high voltage multiplexer ICs. In addition, an integrated amplifier/shaper circuit equipped with either a trapezoidal or 8-fold CDS filtering stage, internal sample and hold, serial analog readout and integrated shaping sequencer is used for device readout. Extremely high speed readout of up to 2 μs per row is possible with these circuits.

1.3 Macropixel devices

For pixel sizes larger than $\sim 150 \times 150\ \mu\mathrm{m}^2$, the realization of a CCD based sensor becomes increasingly difficult, as the charge transfer slows down as it becomes more and more dependent on diffusion due to large equipotential areas underneath the register contacts, and the required potential differences between the registers to create a reasonable drift field become larger. Arbitrarily large pixel sizes can be achieved, however, by merging the concept of a silicon drift detector (SDD) with a DEPFET type readout amplifier. By surrounding the DEPFET cell with an SDD-like driftring structure, the pixel size can be adapted to the requirements by simply changing number, size and geometry of the drift electrodes [10]. In the volume of an SDD device controlled by the driftring

2009 JINST 4 P03012

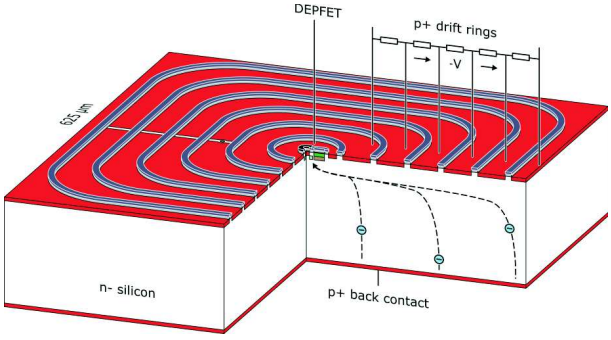

Figure 4. Cross-cut through a Macropixel device. By replacing the readout anode of a conventional SDD with a DEPFET, charge storage capability can be added to an SDD array. In this way, large integrating imaging detectors can be built from an array of Macropixels.

structure, a potential cascade is superimposed on the reverse bias to create a drift field, which drives the electrons towards the central readout anode. In this way, the pixels can be made arbitrarily large, while the capacitance of the readout node remains constant. Replacing the readout anode of the SDD with a DEPFET cell, the DEPFET's charge storage capability is combined with the scalability of the SDD arrangement (see figure 4). The resulting device, henceforth referred to as macropixel, has the combined benefits of DEPFET and SDD. The pixel size is arbitrarily scalable changing number, geometry and size of the drift rings. By integration of an array of square SDD devices on a common bulk yields a large area FPA, which can be read out row-by-row on-demand due to the DEPFET's charge storage capability. As the DEPFET is powered only in case it is actually read out, a macropixel matrix is very power efficient, and like for any sideways depleted detector, the backside radiation entrance window is homogeneous and has a fill factor of 100%. Due to the low input capacitance of the DEPFETs, the devices can be read out very fast at low noise, and as no charge transfer is required, the DEPFET devices are intrinsically more radiation hard than comparable CCD devices. The radiation hardness of the DEPFET technology has already been proven experimentally. These properties make DEPFET macropixel matrix devices (MPDs) suitable for a large number of experiments. Single macropixel prototypes from an earlier prototyping run have successfully tested and showed outstanding performance in spite of the large pixel area.

2 The eROSITA instrument

Being part of the payload of the new SRG (Spectrum-Röntgen-Gamma)-Satellite [13], the eROSITA (extended Roentgen Survey with a Telescope Array) mission is designed to meet two primary scientific goals: Firstly, the ROSAT imaging all-sky survey is to be extended to higher X-ray energies up to 10 keV with unprecedented spectral and angular resolution [12]. Hereby, eROSITA is a pathfinder mission for the large, next geneneration X-ray observatories, particularly SIMBOL-X and IXO. Secondly, by detection of a sufficiently large number of clusters of galaxies, precise measurements will be feasible of the equation of state of Dark Energy and of "baryonic acoustic oscillations" in the power density spectrum of galaxy clusters.

The required detection efficiency for this task will be provided by the eROSITA instrument, which consists of an array of seven imaging telescopes (see figure 5). Each telescope consists

2009 JINST 4 P03012

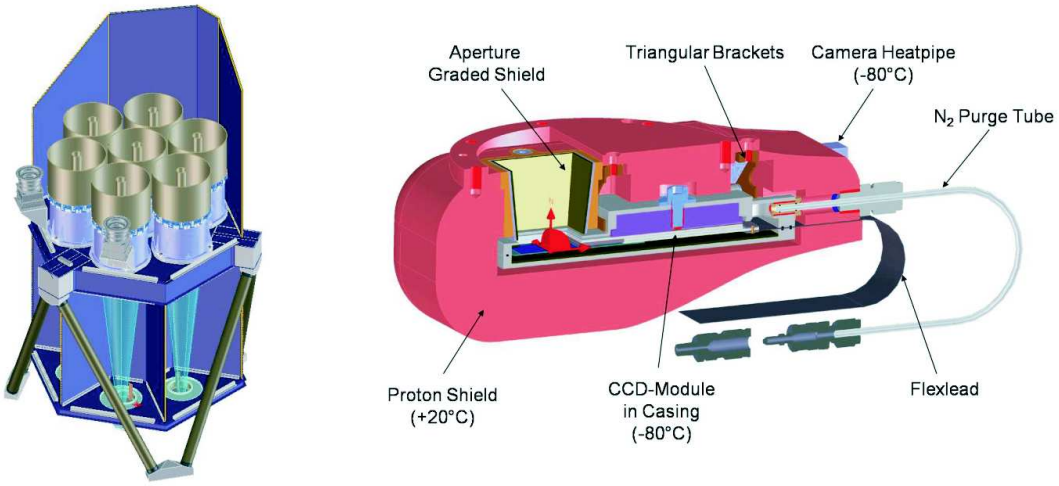

Figure 5. Setup of the eROSITA instrument (left) and the pnCCD camera module (right). The eROSITA instrument consists of a telescope array of 7 Wolter Type 1 X-ray telescope consisting of 54 nested mirror shells. Each telescope has its individual pnCCD module as focal plane detector. The overall field of view is 1°, the projected half energy width of the modules is ∼15 arcsec. The right part of the figure shows a cross section of an eROSITA camera module. X-rays enter the pnCCD image area top left through the cut-out in the proton shield. While the copper proton shield is not cooled, the camera casing, which surrounds the CCD detector, is connected via a heat pipe to the central cooling system for all seven cameras.

of a highly nested mirror system with 54 paraboloid-hyperboloid mirror shells and a frame store pnCCD camera with a 3×3 cm^2 large image area. The pnCCD allows spectroscopy of X-rays with a quantum efficiency of at least 90% up to an energy of 11 keV.

The pnCCD detector for eROSITA is based on the pnCCD developed for XMM-Newton and upon the frame store pnCCD designed for the proposed DUO mission. A schematic view of the CCD is shown in figure 6, together with a photo of an assembled laboratory module. According to the scientific requirements of eROSITA, the detector provides a field of view of 1° in diameter, which is composed of 384×384 pixels with a size of $75\ \mu\text{m} \times 75\ \mu\text{m}$. The energy of the X-ray photons is precisely measured with a readout noise of 2-3 electrons ENC.

A relatively high time resolution is required for eROSITA due to the high scan rate during the all-sky survey. In the planned low earth orbit (LEO) with altitude of 580 km, a frame rate of 20 images/s for the camera is necessary to avoid a loss of angular resolution of the X-ray optics. If very bright sources are observed, the short exposure time of 50 ms minimizes the probability of photon pile-up in a pixel of a frame as well. After the 50 ms exposure time the image is rapidly transferred to the frame store area within 200 μs. As the frame store area is shielded against X-rays, the stored image can be read out without interference row by row, while the photons of the next image accumulate in the image area. The readout time, i.e. the time to process the image information integrated during the exposure time, is less than 10 ms for the complete image. During the remaining time the CAMEX (CMOS Amplifier and MultiplEXer) readout IC is switched in standby mode to minimize the average heat dissipation to the focal plane.

The fast, low-noise readout is done by fully column-parallel signal processing in the pnCCD and the analog readout ASIC CAMEX. The pixel size of $75\ \mu\text{m} \times 75\ \mu\text{m}$ was matched to the

2009 JINST 4 P03012

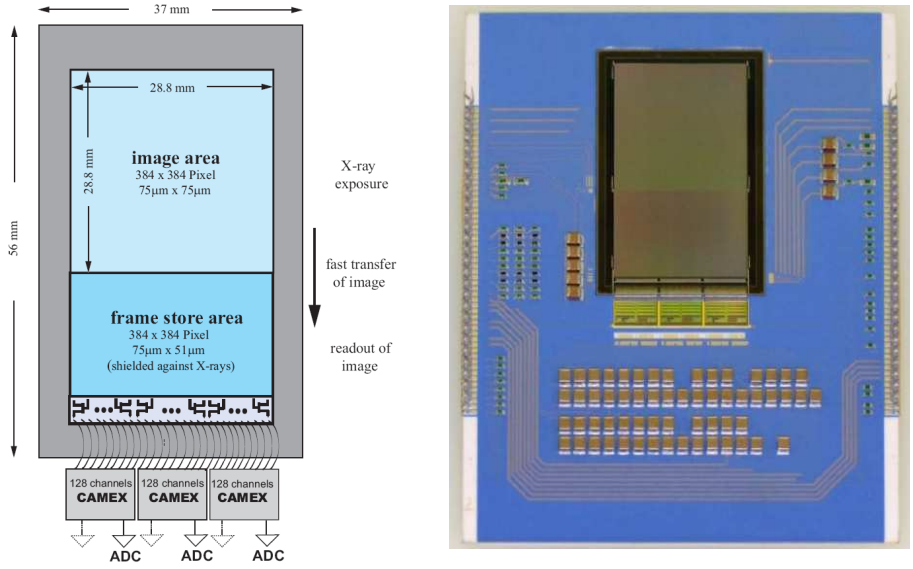

Figure 6. Schematic view of an eROSITA pnCCD (left). The imaging area consists of 384 $\times$ 384 pixels of 75 $\times$ 75 μm^2 size. The charge can be rapidly transferred to the frame store region, consisting of an equally dimensioned array with different pixel size (75 $\times$ 51 μm^2). This region is shielded against X-rays. Readout of the image stored in the frame store region is done in a column-parallel way by three 128 channel VLSI low-noise shaper/amplifier ICs of the CAMEX type. To the right, a photo of a prototype ceramic hybrid equipped with CCD sensor and readout ASICS is shown.

projected resolution of the mirror system of 15 arcsec half energy width (HEW) on-axis. The incidence positions of the X-ray photons on the detector can be determined with a higher level of spatial accuracy by analyzing the patterns of charge distribution between the pixels. As the CCD is sidewards depleted device, its bulk is sensitive over its entire 450 μm of thickness, and the backside provides for a homogeneous, ultra-thin entrance window. The large bulk thickness extends the quantum efficiency to the higher energy x-ray region up to 11 keV, where a quantum efficiency of 90% is expected. The ultra-thin, homogeneous pn-junction on the backside serving as photon entrance window provides for a quantum efficiency close to 100% for all X-ray energies down to 0.3 keV. Moreover, the response is homogeneous over the entire image area, as the fill factor of the backside is 100%. As a certain degree of suppression of optical and UV light is necessary in space for high-resolution spectroscopy, a filter system was deposited directly on the photon entrance window of the CCD. This 0.17 μm thick filter layer stack, composed of silicon oxide, silicon nitride and aluminum reduces the QE at energies below 1 keV. Whereas at 0.9 keV energy a QE of 90% is still obtained, it decreases for 400 eV photons to 60% and at 300 eV to 38% for the detector including filter. But even with this expected decrease the QE is still better than the QE of a system providing a comparable degree of optical and UV attenuation by means of an external filter.

To evaluate the properties of the CCD devices, tests were done on prototypes like the one shown in figure 6. Some results from the first measurements are shown in figure 7. A readout noise of 2.4 electrons was obtained for the later eROSITA operating conditions. The device was operated with a frame rate of 20 images/s and a temperature of -80° C. The intensity image measured with an ^{55}Fe source shows an insignificantly small number of pixel defects. The imaging capabilities of

2009 JINST 4 P03012

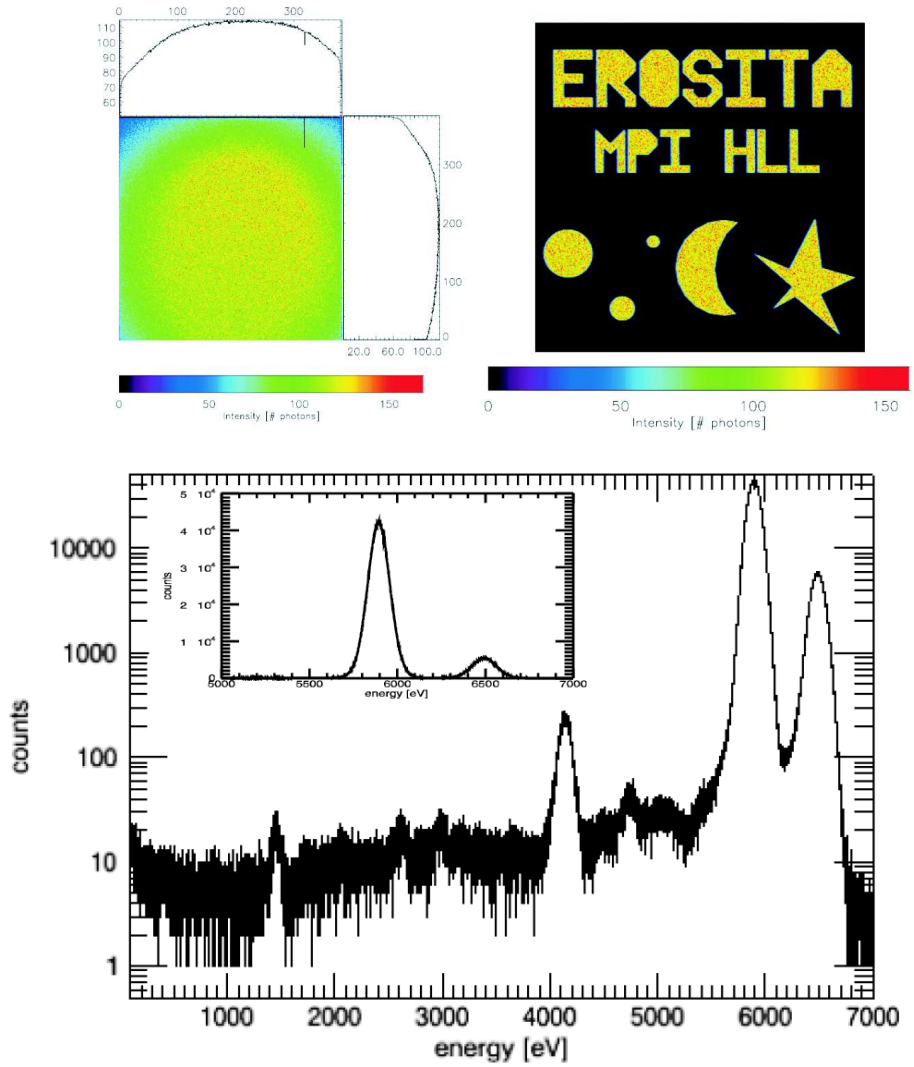

Figure 7. Results from first prototype tests of eROSITA pnCCD devices. Upper left: The flat field illumination with an ^{55}Fe source shows the excellent spatial homogeneity of the device. The observed inhomogeneity is due to the large detector size and the short distance between source and detector. Only one point defect, a non-transferring pixel, can be observed in the upper right corner of the device. The resulting energy spectrum is shown in the lower part of the figure with a logarithmic scale for number of counts and an inset with linear scale. The Mn-K$_\alpha$ and Mn-K$_\beta$ lines at 5.9 keV and 6.5 keV are observed, with a FWHM of 133 eV @ 5.9 keV for single events and 143 eV for all events. The peak-to-background ratio of 7700:1 was determined referring to the Mn-K peak and the average number of counts between 0.4 keV and 1 keV. The expected silicon escape peak at 4.2 keV appears due to the use of silicon as detector material. The additional peak at 1.5 keV results from Al fluorescence X-rays, which were mainly generated in the Al-housing of the source. Illuminating the sensor with 1.5 keV X-rays (Al-K) using a patterned silicon baffle yields the image shown in the top right corner.

the device are demonstrated illuminating the device with Al-K photons (1.5 keV) of an X-ray tube through a patterned silicon baffle place in front of the CCD. The image quality is impressive, especially the strong suppression of 'out-of-time' event occurrence, which is a benefit of the frame store

2009 JINST 4 P03012

architecture. Spectroscopic analysis of the first ^{55}Fe data sets yields for the Mn-K$_\alpha$ line at 5.9 keV an energy resolution of 133 eV FWHM for single events (i.e. signal charge collected in one pixel) and 143 eV FWHM on average for all event patterns. A measurement with high photon statistics revealed an excellent peak-to-valley ratio of 7700:1. The minimum occurrence of partial events (i.e. events resulting from incomplete signal charge collection) also proves the excellent quality of the radiation entrance window, as recombination of electron-hole pairs within the non-depleted part of the entrance window implantation is the main source of incomplete charge collection.

3 The Low Energy Detector for SIMBOL-X

SIMBOL-X is a joint French-Italian-German scientific X-ray mission with a projected launch date mid 2014 [15]. The mission's core targets are the census and physics of black holes and the mechanisms of cosmic particle acceleration. The scientific tasks require a high sensitivity over a broad energy band which is obtained by the application of new technologies. SIMBOL-X will be the first mission using a focusing telescope at X-ray energies well above 10 keV where up to now only imaging systems using collimators (e.g. BeppoSAX PDS) and coded mask apertures (e.g. INTEGRAL IBIS/ISGRI) have been available. In this way a sensitivity level will be reached which is improved by three orders of magnitude with respect to INTEGRAL and equivalent to XMM Newton in the soft X ray band. The SIMBOL-X telescope is based on a Wolter type-I geometry with 100 nested Ni mirror shells with diameters from 26 cm to 65 cm. The large on-axis effective area ($>$ 1000 cm^2 at 2 keV, $>$ 300 cm^2 at 30 keV, and $>$ 100 cm^2 at 75 keV) is obtained by high-reflectivity multi-layer coating of the mirror surfaces and by an extreme focal length of 20 m. The field of view (FoV) is 12 arcmin and the targeted angular resolution is 20 arcsec HEW. For temperature stabilization, the telescope's entrance and exit sides are covered with thermal blankets defining the low-energy cut-off at 500 eV. To reduce the background by low-energy protons which would reach the focal plane through the telescope the support structure of the mirror shells is equipped with permanent magnets deflecting protons with energies $<$ 300 keV.

As a telescope with 20 m focal length and its focal plane instrumentation cannot be housed in a single spacecraft structure, SIMBOL-X will be the first mission to adopt the formation flight of two independent mirror and detector spacecrafts (see figure 8). Both spacecrafts are aligned by an active control system to provide the formation flight with a relative position accuracy of 1 cm^3. The two SIMBOL-X spacecrafts will be launched as a single stack by a Soyuz-Fregat carrier from Kourou to a high eccentric 4-days orbit with a perigee of 20.000 km and an apogee of 180.000 km. The mission duration is planned to be two years of effective science time plus the provision for an extension of two calendar years.

The focal plane instrumentation has to cover the energy band from 500 eV to 80 keV with a required spectral resolution E/ΔE of 40 - 50 in the energy range from 6 - 10 keV and around 50 at 60 keV. As there is no single detector system capable of providing this performance, the SIMBOL-X focal plane is equipped with two imaging spectroscopy systems for the soft (low energy detector (LED)) and the hard (high energy detector HED) energy band. The telescope's usable FoV in the LED energy range is 12 to 15 arcmin. At a focal length of 20 m this corresponds to a circle with 7 to 8.8 cm in the focal plane. To display the complete FOV, both focal plane detectors, LED and HED, will have a sensitive area of 8 $\times$ 8 cm^2 each. The angular resolution of the telescope is 20 arcsec

2009 JINST 4 P03012

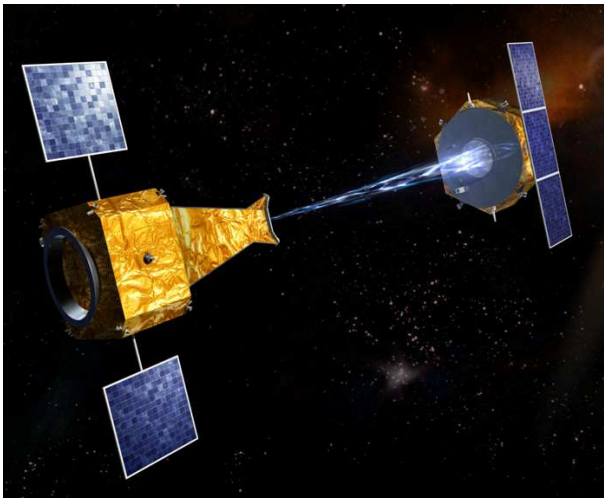

Figure 8. Artist's view of the SIMBOL-X spacecrafts. Mirror system and scientific instrumentation are located on two individual spacecrafts being positioned by an autonomously working active position control system to an accuracy of ≤ 1 cm^3.

HEW. At a focal length of 20 m this corresponds to a point spread function of 1.9 mm in the focal plane. To avoid undesired oversampling by too small pixels on one side, and to maintain a position resolution well below the limitation of the telescope, the pixel size of both focal plane detectors, LED and HED, has been chosen to be 625×625 μm^2. That way the HEW is roughly an area of 3×3 pixels, which is sufficient for reliable position reconstruction. The LED must be sensitive for energies transmitted by the telescope's thermal blankets (≥ 500 eV) requiring a thin entrance window with high quantum efficiency for soft X rays. The upper limit of the LED sensitivity is given by the absorption properties of silicon which is getting 'transparent' for energies beyond 20 keV. Among other science targets, SIMBOL-X intends to investigate matter under the extreme conditions of accretion on compact massive objects by measuring energy-shifted characteristic emission lines. The analysis of the spectra requires an energy resolution of ≤ 150 eV FWHM at 5.9 keV, corresponding to an ENC of 10.5 electrons r.m.s. To keep the dead-time caused by the anticoincidence connection of the three detector systems (LED, HED, AC) low the LED must be read out extremely fast with a frame rate of 8 kHz. The observation of variable objects with quasi-periodic oscillations in the msec-range requires a time resolution of 50 μsec. This is achieved by a window mode which does not read the full frame but only the sensor region containing the object with higher repetition rate. As the LED is placed in front of the HED it must be fully sensitive over the entire area and homogeneously transparent for hard X rays. Consequently, the LED must be a monolithic device without support structure that would cause a shadow on the HED in the FOV. Due to the limited resources of the detector spacecraft the LED must operate at a relatively warm temperature of nominal 45 °C. That is only feasible with a detector process yielding an extremely low leakage current level with enough headroom for radiation related degradation during the mission lifetime. At the beginning of the SIMBOL-X project there was no known detector fulfilling all requirements simultaneously. Therefore, the development of the DEPFET based MPDs has been initiated at the MPI semiconductor laboratory.

2009 JINST 4 P03012

Seen from the telescope, the High Energy Detector (HED) is placed behind the LED and detects only hard X rays transmitted through the LED, as due to the small atomic number of silicon the LED efficiency drops steeply at energies > 10 keV. In an energy band from 5 keV to 80 keV the respective efficiencies of LED and HED sum up to 100 %. The High Energy Detector (HED) is a pixelated Schottky-type cadmium-telluride detector with a sensitive area of 8×8 cm^2 and a pixel size of 625×625 μm^2. The HED architecture follows a modular concept. The smallest subunit has a 1 cm^2 crystal with 16×16 pixels. The CdTe crystal with a thickness of 1 - 2 mm is bump bonded on the 3D integrated readout electronics cuboid called CALISTE and containing readout ASICs of the IDeF-X type [14]. Each pixel has its own electronics chain. The full focal plane detector is built of an 8×8 array of CALISTE modules. The readiness of this technology has been demonstrated by a smaller prototype module with 8×8 pixels providing an excellent energy resolution of 0.78 keV FWHM at 59.5 keV and 37 °C. As SIMBOL-X is aiming at the discovery and study of faint sources, the detector background must be at an extremely low level of $2 - 3 \times 10^{-4}$ cts/(cm$^2 \cdot$ sec $\cdot$ keV). To achieve this performance it is necessary to enclose the imaging detectors by the combination of a graded absorber shield and an active anticoincidence shield. The active anticoincidence detector (AC) is a compact 'box' of plastic scintillators (BC 400) covering all possible directions for incident high-energetic particles or photons except the telescope FoV. In addition to the active anticoincidence shield the background is also reduced by graded shield absorbers. The passive shield has three components: graded shield plates covering the scintillators, a 2 m long collimator on top of the focal plane assembly and a sky shield surrounding the telescope on the mirror spacecraft. The focal plane architecture is driven by the requirement to integrate the LED and HED detection planes within a vertical distance of ≤ 1 cm to avoid imaging errors. A sketch of the payload design is shown in figure 9.

The MPD for the SIMBOL-X LED with its sensitive area of 8×8 cm^2 will be the largest monolithic sensor for X ray imaging spectroscopy, almost filling the usable area of a 6 inch wafer [10]. The wafer thickness is 450 μm. The sensor format is 128×128 with a pixel size of 625×625 μm^2. For redundancy reasons the pixel array is divided into four quadrants with 64×64 pixels, each having individual power supplies and readout and control electronics. This division is purely electrical and not related to insensitive regions on the sensor. The largest part of the pixel area is filled by the drift diode structure consisting of six concentric rings with rounded corners to avoid high-field regions. The outmost ring is common to all pixels of a quadrant. The DEPFET amplifier in the pixel center is implemented in the standard design for X-ray spectroscopy applications with circular outline and the gate dimensions 5 μm length and 47 μm width. For the SIMBOL-X LED there are two baseline readout modes:

- Full Frame Mode: The four quadrants are read simultaneously row by row. The operations for all pixels within one row are performed in parallel. The frame time is given by the time required to process the signal of one pixel, which will be presumably 4 μs, corresponding to a frame rate of 4 kHz for a device with 64 pixel rows. To speed up system readout, two pixel rows per quadrant will be read simultaneously, thus reducing the full frame time by a factor of two but also doubling the number of readout channels.

- Window Mode: The MPD concept allows to address arbitrary sub-areas of the pixel array down to single pixels. However, this full flexibility requires a complex on-chip wiring and

2009 JINST 4 P03012

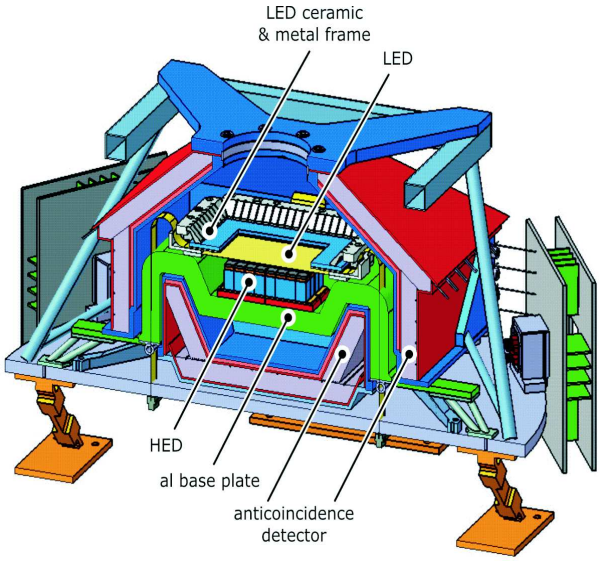

Figure 9. Sketch of the SIMBOL-X instrumentation payload. The LED is located directly behind the aperture, while the HED is located behind the LED. Both instruments are mounted on an AL baseplate, which is connected to the spacecraft radiators by heatpipes. The detector stack is surrounded by active and passive graded absorber shields. The active shield consists of an anticoincidence detector using a plastic scintillators being read out with photomultipliers.

control logic. Therefore, for the SIMBOL-X LED only one basic window mode for the observation of bright point sources has been conceived. In window mode only a part of the pixel array is read starting from the equatorial center line towards north and south directions. The vertical window position is centered on the equator line of the sensor area. The number of rows in the window is selectable. In the east/west direction the window has the full width of the sensor area.

Due to the large pixel size ($625 \times 625\ \mu m^2$) and the long integration time ($\gg 100\ \mu s$) the energy resolution will be clearly limited by the leakage current. The typical value obtained by the DEPFET technology is < 1 nA/cm^2 at room temperature and full depletion of a 450 μm thick device. Scaling this extremely low value to the SIMBOL-X operation conditions, an energy resolution of 130 eV (FWHM at 5.9 keV) is expected at the beginning of the mission. This performance provides a large enough buffer for the additional leakage current caused by radiation damage in the orbit. By simulation an integrated fluence of 3×10^8 / cm^2 of 10 MeV equivalent protons during a mission time of five years has been estimated. The effect of one proton has been measured in a dedicated irradiation campaign to be an additional amount of leakage current of 2.4×10^{-17} A at room temperature allowing for the LED operation within the SIMBOL-X specifications (< 150 eV FWHM at 5.9 keV) throughout the full mission life time. The LED quantum efficiency at the low energy end of the SIMBOL-X energy band is a function of the detector entrance window and of absorbing layers in front of the detector. As the LED has an optical burden of $> 10^5$ photons per pixel and frame imposed by the autonomous alignment system of the two spacecrafts the presence of an optical filter is mandatory. It is foreseen to deposit an aluminum layer of 100 nm thickness directly on the sensor's entrance window attenuating the optical load by a factor 10^6 but also re-

2009 JINST 4 P03012

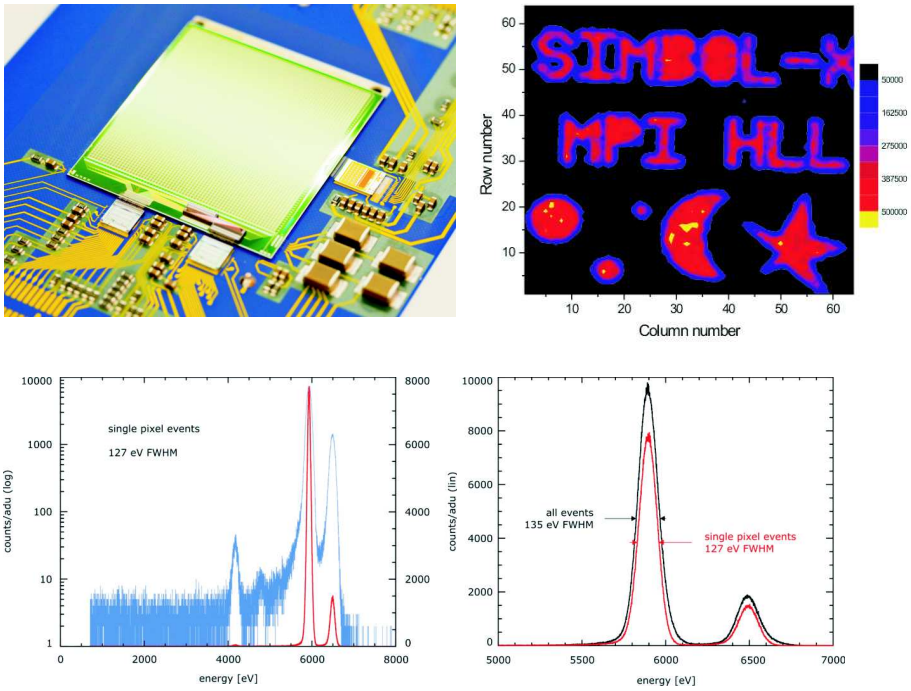

Figure 10. Photo (top left) and results from tests of a prototype of the SIMBOL-X LED MPD. The device consists of 64 $\times$ 64 pixels with an area of 500 $\times$ 500 μm^2 each. The overall sensitive area is 3.2 $\times$ 3.2 cm^2. The control- and readout electronics required to operate the device are visible at the lower right (CAMEX IC) and lower left (2 $\times$ Switcher IC) edges of the sensor respectively. Sensor and ICs are integrated onto a ceramic thick-film hybrid. The device was operated at -90°C at a framerate of $\approx$ 700 Hz. The spectra obtained by illumination with an ^{55}Fe source display an energy resolution of 127 eV FWHM for single events and 135 eV for all events, and an excellent peak-to-background ratio of 3000:1. The readout noise was 3.1 electrons ENC. Illumination through a patterned silicon baffle (top right) demonstrates the homogeneity and imaging capability of the device.

ducing the low energy response of the LED. The quantum efficiency will still be above 80 % in the energy interval from 0.7 to 13 keV. Towards high energies the LED quantum efficiency is limited by the poor absorption of silicon and the device thickness of 450 μm. From 20 keV on the LED will be almost transparent and all more energtic photons are absorbed by the hard energy detector.

To demonstrate the readiness of the DEPFET-MPD technology a representative prototype of a SIMBOL-X LED quadrant has been processed and qualified. The quadrant prototype has the same format of 64 $\times$ 64 pixels but a smaller pixel size of 500 $\times$ 500 μm^2. With its sensitive area of more than 10 cm^2 it is the largest monolithic X ray imaging spectrometer since the pnCCD camera of XMM Newton. The room temperature leakage current level has been measured to be 100 pA/cm^2 at full depletion of the 450 μm thick device. The prototype has been mounted on a ceramic board and wire bonded to the CAMEX and SWITCHER front-end chips. The sensor has been tested in vacuum conditions in spectroscopy mode using an ^{55}Fe source. Due to limitations in the readout system and in the thermal setup the sensor has been operated at lower temperature (-90 °C) and at lower frame rate ($\sim$ 700 Hz) compared to the SIMBOL-X conditions. Nevertheless, the results are scalable with temperature and readout time so that full compliance with the requirements is

2009 JINST 4 P03012

achieved. The sensor has been found to be defect-free and homogeneous. The overall electronic noise is 3.1 electrons ENC. The energy spectrum of an ^{55}Fe flat field illumination shows an energy resolution of 127 eV FWHM at 5.9 keV for single pixel events and 135 eV for all events including reconstructed multiple pixel hits and a peak-to-background ratio of 3.000 : 1. The imaging capability of the system has been demonstrated by the shadow image of a patterned silicon mask. An image of a prototype module and selected results are shown in figure 10.

4 The MIXS focal Plane assembly on BepiColombo

ESA's 5th cornerstone mission BepiColombo is named after the Italian engineer and mathematician Guiseppe "Bepi" Colombo. It is is a planetary exploration mission to Mercury to be operated by the European Space Agency ESA in collaboration with the Japanese Space Agency JAXA [16]. Being a successor to NASA's simpler MESSENGER (MErcury Surface, Space ENvironment, GEochemistry and Ranging) probe, BepiColombo will study the origin and evolution of a planet in close proximity to the parent star, study Mercury as a planet, its form, interior, structure and geology, its surface composition and craters, investigate the traces of Mercury's vestigial atmosphere and its magnetosphere.

In 2013, the BepiColombo Mercury Composite Spacecraft (MCS) will be sent to its 6 years' journey to Mercury. Upon arrival at Mercury in 2019, two independent probes, the Mercury Magnetospheric Orbiter (MMO) and the Mercury Planetary Orbiter (MPO), will be deployed in two independent polar orbits around the planet. The envisaged mission lifetime is one year, with a possible extension for another year.

Each spacecraft carries an individual set of instrumentation. While the MMO will study Mercury's magnetosphere and exosphere, and the interactions within the system Mercury-Sun, the MPO will mainly focus on observing the crust of Mercury. A large part of its instrumentation is made to do multi-wavelength scans of the entire Mercury surface. One of the instruments on board the MPO is the so-called MIXS (Mercury Imaging X-ray Spectrometer) instrument, which will perform a planetary XRF analysis of Mercury's crust with unprecedented spectral and spatial resolution [17]. The technique of planetary XRF makes use of the fact that in absence of a shielding atmosphere the coronar X-rays from the sun directly illuminate the planet's surface and generate characteristic X-ray fluorescence radiation, a quantitative measurement of which can be used to determine the elemental abundance on the surface. In case of Mercury, especially the concentration of the important tracer elements Magnesium, Silicon, Aluminum and Iron within the crust are of interest. As the quantitative interpretation of the measurement results strongly relies on the availability of reliable data about the spectrum and intensity of the coronar X-rays, MIXS depends on the reference data about the solar input flux provided by Solar Intensity X-ray Spectrometer (SIXS). For the interpretation of the gathered data, MIXS will work closely together with all other MPO instruments. The data will be combined to achieve MIXS' primary scientific objectives. MIXS will measure the average composition of Mercury's crust, determine the compositions of the major terrains, determine the composition inside craters and crater structures and detect iron globally and locally.

Planetary XRF instruments have been used on a variety of missions, with different instrument concepts. Most instruments, e.g. the X-ray spectrometer onboard MESSENGER, use collimated gas proportional counters as X-ray detectors. Due to their limited energy resolution of $\sim$ 880eV

2009 JINST 4 P03012

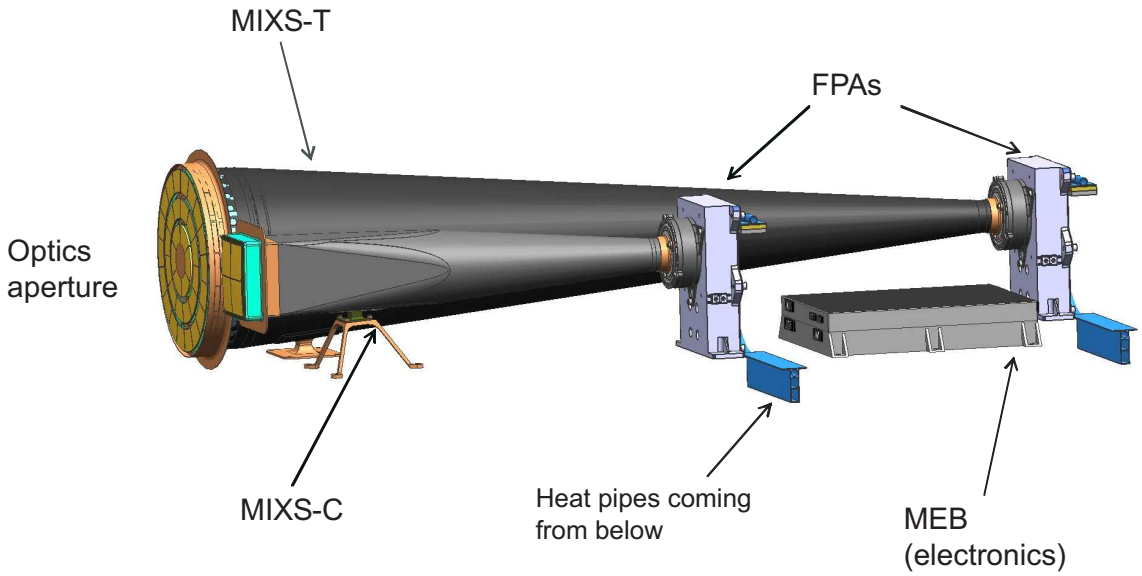

Figure 11. Sketch of the MIXS instrument on BepiColombo. Two channels, one equipped with a high resolution X-ray telescope and one with a collimator optics, with the same focal plane array, are located on a common optical bench and controlled with a common readout electronics. MIXS-C, the collimator instrument, serves for large scale observations of a large footprint in case of low solar X-ray intensity. MIXS-T, which requires higher solar X-ray fluxes, is used for imaging the fluorescence radiation of the surface, capable of resolving features in the sub-kilometer range. The two instrument channels are controlled by a common electronics, located in the MIXS electronics Box (MEB).

FWHM at 5.9 keV, shell emission lines of Mg (1.25 keV), Al (1.49 keV) and Si (1.74 keV) can not be separated with such an instrument, and the differential X-ray attenuation of three independent instrument channels equipped with filters is used in that energy range. The sensitivity to Iron is limited, as the Iron-K line can be observed only during times with high solar activity, and the Iron-L lines around 700 eV can not be directly observed [19].

MIXS differs radically from previous X-ray instruments for planetary remote sensing, as it will provide for unprecedented spatial and spectral resolution. The excellent spatial resolution is achieved by two complementary channels equipped with optical elements provided by low mass and high efficiency Microchannel Plate (MCP) X-ray optics [18]. For the first channel, MIXS-C, a slumped collimator with a 10° FOV at an aperture of 64×64 mm^2 is foreseen, which is optimized to provide a high throughput of X-rays and ensure that the measurement of major rock forming elements can be achieved for all solar conditions. MIXS-C measurements will be on the scale of 70 to 270 km, sufficient for the separation of the major terrains on Mercury. The second channel, MIXS-T, uses an imaging X-ray telescope of the Wolter type, offering spatial resolutions better than 10 km during periods when the X-ray flux from the surface is sufficiently high, for instance during solar flare events. High spatial resolution provides access to individual landforms such as craters and their internal structures. The MIXS-T telescope will have an aperture of 21 cm, a focal length of 1 m and an effective area of 120 cm^2 @ 1 keV, and 15 cm^2 @ 10 keV. The overall field of view will be 1° for an angular resolution of 1.7 arcmin HEW. Both optic modules will be iridium coated to increase their effective area.

2009 JINST 4 P03012

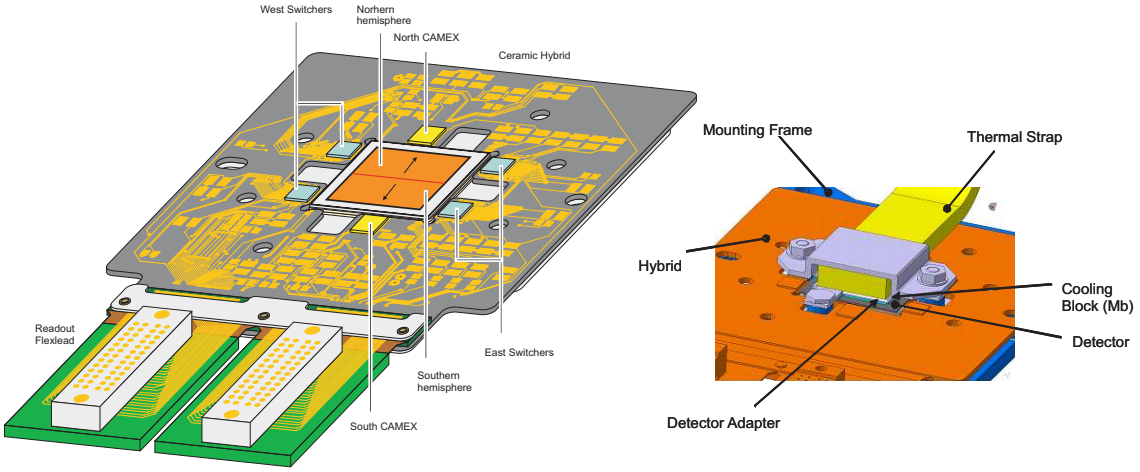

Figure 12. Hybrid schematic and mounting concept for the MIXS FPA. The sensor is divided into two independent hemispheres, each of which having its own control and readout electronics (left). The connection to the electronics is done via a flex circuit. Sensor IC and Hybrid have no direct thermal contact. The thermal connection to the cold finger is done directly to the backside of the sensor, to which the cold finger is attached via an aluminum nitride sensor adapter (right). The 0.5 mm wide vacuum gap between sensor and hybrid, the latter being at spacecraft ambient temperature ($\sim$ +30°C), provides for good thermal decoupling. The heat intake via the bond wires is not negligible, but still small. Thermal simulations predict a temperature below -43° C.

The spectral resolving power is achieved by the use of DEPFET MPDs as sensitive elements in the focal plane assembly (FPA) [20]. For the sake of simplicity, both of MIXS channels are equipped with identical FPAs with one MPD each. The detectors will measure X-rays in the energy band of 0.5 - 7.5 keV. The energy resolution limit and the limit on the electronic noise are, with 200 eV FWHM @ 1 keV and 10 e^- ENC respectively, very moderate. This performance allows the separation of X-ray line emission from elements of interest and provides access to lines not accessible to previous instruments, including the Fe-L emission lines. The sensitive area of 1.9 $\times$ 1.9 cm^2 is made to match the mirror system FOV, and the pixel size of 300 $\times$ 300 μm^2 is again driven by the size of the PSF. This pixel design requires 3 driftrings per pixel, the outermost ring again being common to all pixels. The energy range is selected to cover both the iron-K line (6.4 keV) and the iron-L line (0.71 keV). As mentioned above, a low energy limit of 0.5 keV permits the detection of iron even in case of a quiet sun state using the L-line, which greatly increases the sensitivity on iron. The scientific drivers for the required time resolution of $\leq$ 1 ms are mainly the spacecraft movement over ground and partially also due to dynamics of the incident X-ray intensity. Nevertheless, the system foresees a much higher framerate than 1 kHz, as the fast readout helps to suppress the influence of the increase of leakage current due to radiation damage during the mission lifetime. This is also the reason, why the sensor has been divided into two independent hemispheres similar to the SIMBOL-X LED and is read out to two sides. This additional degree of parallelization increases the readout speed by a factor of two, as shown in figure 12. The setup of the MIXS instrument is shown in figure 11.

The biggest challenge for MIXS is the radiation hardness. The overall proton dose of $\sim$ 3 $\times$ 10^{10} 10 MeV Protons / cm^2 has a big impact on the operating scenario. The expected increase

2009 JINST 4 P03012

of leakage current due to NIEL, which also affects the energy resolution, can only be partially compensated via the readout speed. As the cooling resources on board of MPO are quite limited, the design of the FPA has to be made in a way, that all available cooling power is made available for cooling the detector (see figure 12). Operating temperatures of around -45° C are required on the sensor to keep the required energy resolution. Thermal simulations show, that this temperature can only be achieved in case an extensive thermal decoupling of sensor and front end electronics, requiring an advanced mechanical mounting concept, is applied. In addition, various annealing scenarios are being considered. Furthermore, impact from optical and infrared photons passing through the optics aperture has to be kept low, which is done by additional filters in the optics baffle and an aluminization on the sensor entrance window.

By the time of writing, no MIXS flight grade detectors have been tested yet. But as the design is equivalent to the SIMBOL-X prototypes except for the pixel area, the tests of the SIMBOL-X prototypes can be regarded to be representative for the MIXS detectors as well, and as the pixel area of the prototypes is more than two times larger and the observed yield and their performance has been found to be very good, it is justified to expect good performance and yield figures.

5 Outlook: The International X-ray Observatory IXO

The large, next-generation X-ray observatory, the International X-Ray Observatory IXO, is going to be a joint enterprise of ESA, JAXA and NASA which is currently been studies as a merged successor project of the ESA/JAXA XEUS mission and NASA's Constellation-X mission. High sensitivity instrumentation with high spectral resolution together with a mirror system with large effective area are essential for achieving its primary science objectives. IXO will study growth and evolution of supermassive black holes, and will use them as a test system for the predictions of general relativity. It will study galaxy formation and galaxy cluster evolution and study the influence of dark matter and dark energy. It will be used to investigate element and planet formation as well as particle acceleration mechanisms in the universe. The starting configuration for IXO, which is currently under study, foresees a single platform with one large X-ray mirror and an extensible optical bench with a 20-25m focal length, with an interchangeable focal plane. The current payload instrumentation foresees an X-ray wide field imaging spectrometer (WFI) combined with an high energy detector (HED), a high spectral resolution non-dispersive X-ray spectrometer with smaller FOV (Narrow-Field Imager NFI), which is likely to be a cryogenic TES, and an X-ray grating spectrometer. In addition, allocation for further payload elements with modest resource demands is being studied, such as an X-ray polarimeter and a high time resolution instrument to study variable X-ray sources with great timing accuracy.

The FOV of IXO will cover 18 to 20 arcmin, depending on the focal length which will be finally implemented. The current proposal for the WFI foresees an instrument very similar to the former XEUS WFI [21] capable of covering this entire field of view. The WFI will provide imaging capabilities with near Fano-limited performance and do a pre-characterization of interesting sources to be studied further with the high resolution non-imaging or narrow FOV instruments respectively. It will consist of a DEPFET MPD with $\sim 1 \times 10^6$ pixels of $100 \times 100\ \mu m^2$ size located on a six inch wafer with a common homogeneous backside. This device will cover the entire usable region of the wafer. As shown in figure 13, the sensor will be surrounded by the control- and readout

2009 JINST 4 P03012

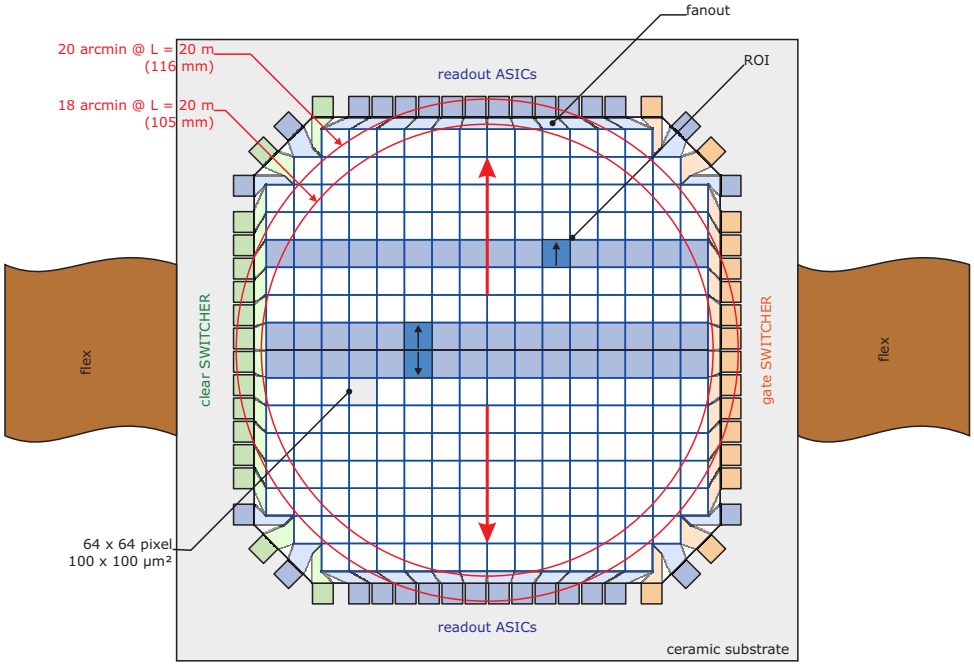

Figure 13. Sketch of the proposed IXO WFI. It will consist of a $\sim 1 \times 10^6$ pixel DEPFET MPD integrated monolithically on a six inch wafer and nearly filling its entire usable area. The WFI will be surrounded by its control- and readout electronics. Its two hemispheres will be read out independently. Random access to on-the-fly selectable ROIs, e.g. in case multiple bright objects will have to be observed simultaneously, will be one of the instruments key features.

electronics. Again, the sensor is divided into two hemispheres, which are, for improved readout speed, read out in parallel. As a new feature, the WFI will allow to allocate and address arbitrarily large regions of interest (ROIs) on the sensor on the fly, and read them with increased repetition rate and unchanged spectral performance, e.g. to observe multiple bright objects distributed over the FOV. This readout mode makes excessive use of the DEPFET's random pixel access capability. The envisaged row processing time for the WFI is around 2 μs, which yields a framerate of 1 kHz, but the time resolution can be much better than 1 ms in case of an ROI based observation, depending on the size of the ROI, e.g. 32 μs in case a 16 row wide ROI is selected. The accomodation of the Hard X-ray detector behind the WFI, forming a SIMBOL-X like instrumentation stack, is currently being investigated. Prototype sensors for the WFI recently produced at the MPI semiconductor laboratory in Munich are about to undergo testing especially with respect to high speed readout and the windowing capabilities [22].

References

[1] E. Gatti and P. Rehak, *Semiconductor drift chamber — An application of a novel charge transport scheme*, *Nucl. Instrum. Meth.* **A225** (1984) 608.

[2] P. Lechner et al. *The Wide Field Imager of the European X-Ray Observatory*, *IEEE Nucl. Sci. Symp. Conf. Rec.* **3** (2006) 1595.

2009 JINST 4 P03012

[3] N. Kimmel et al., *Analysis of the charge collection process in pnCCDs*, *Proc. SPIE* **6276** (2006) 62760D.

[4] L. Strüder et. al., *The European Photon Imaging Camera on XMM-Newton: the pn-CCD camera*, *Astron. Astrophys.* **365** (2001) L18.

[5] N. Meidinger et al., *Fast large-area spectroscopic and imaging CCD detectors for X-ray astronomy with eROSITA and for exploration of the nanocosmos*, *Proc. SPIE* **6686** (2007) 66860H.

[6] J. Kemmer and G. Lutz, *New Detector Concepts*, *Nucl. Instrum. Meth.* **A 253** (1987) 365.

[7] L. Strüder et al., *XEUS wide field imager: first experimental results with the x-ray active pixel sensor DEPFET*, *Proc. SPIE* **5165** (2004) 10.

[8] J. Treis et al., *DEPMOSFET Active Pixel Sensor Prototypes for the XEUS Wide Field Imager*, *IEEE Trans. Nucl. Sci.* **52** (2005) 1083.

[9] G. Lutz et al., *New DEPFET structures: Concepts, Simulations and Experimental Results*, *Proc. SPIE* **7021** (2008) 70210Y.

[10] C. Zhang et al., *Development of DEPFET Macropixel Detectors*, *Nucl. Instrum. Meth.* **A 568** (2006) 207.

[11] P. Lechner et al. *The Low Energy Detector of SIMBOL-X*, *Proc. SPIE* **7021** (2008) 702110.

[12] P. Predehl et al., *eROSITA*, *Proc. SPIE* **6686** (2007) 668617.

[13] M. Pavlinski et al., *Spectrum-RG/eROSITA/Lobster astrophysical mission*, *Proc. SPIE* **6266** (2006) 62660O.

[14] A. Meuris et al., *Caliste 64, an Innovative CdTe Hard X-ray Micro-Camera*, *IEEE Trans. Nucl. Sci.* **55** (2008) 778.

[15] P. Ferrando et al., *SIMBOL-X: Mission overview*, *Proc. SPIE* **6266** (2006) 62660F.

[16] A. Anselmi and G.E.N. Scoon, *BepiColombo, ESA's Mercury Cornerstone Mission*, *Planetary and Space Science* **49** (2001) 1409.

[17] J. Carpenter et al. *The Mercury Imaging X-ray Spectrometer's (MIXS's) contribution to our understanding of Mercury*, *Planetary and Space Science*, Article in press.

[18] G. Fraser et al., *X-ray focusing using square-pore microchannel plates: First observation of cruciform image structure*, *Nucl. Instrum. Meth.* **A 324** (1993) 404.

[19] C.E. Schlemm et al., *The X-ray Spectrometer on the MESSENGER Spacecraft*, *Space Sci. Rev.* **131** (2007) 303.

[20] J. Treis et al., *DEPFET based X-ray Detectors for the MIXS Focal Plane on BepiColombo*, *Proc. SPIE* **7021** (2008) 70210Z.

[21] The XEUS Instrument Working Group, *X-Ray Evolving Universe Spectroscopy-The XEUS Instruments*, ESA SP-1273 (2003).

[22] J. Treis et al. *Advancements in DEPMOSFET device developments for XEUS*, *Proc. SPIE* **6276** (2006) 627610.

2009 JINST 4 P03012